EXAFS and XANES investigation of (Li, Ni) codoped ZnO thin films grown by pulsed laser deposition

EXAFS and XANES investigation of (Li, Ni) codoped ZnO thin films grown by pulsed laser deposition

Lorenzo Mino, Diego Gianolio, Fabrizio Bardelli, Carmelo Prestipino, E. Senthil Kumar, F. Bellarmine, M. Ramanjaneyulu, Carlo Lamberti and M. S. Ramachandra Rao

J. Phys.: Condens. Matter **25** (2013) 385402 (7pp)

Doi: 10.1088/0953-8984/25/38/385402

EXAFS and XANES investigation of (Li, Ni) codoped ZnO thin films grown by pulsed laser deposition

Lorenzo Mino[1], Diego Gianolio[2], Fabrizio Bardelli[3], Carmelo Prestipino[4], E. Senthil Kumar[5], F. Bellarmine[5], M. Ramanjaneyulu[5], Carlo Lamberti[1] and M. S. Ramachandra Rao[5]*

[1]Department of Chemistry, NIS Centre of Excellence, and INSTM Reference Center, University of Turin, via P. Giuria 7, 10125 Torino, Italy
[2]Diamond Light Source Ltd., Harwell Science and Innovation Campus, Didcot OX11 0DE, United Kingdom
[3]Institut des Sciences de la Terre, Université Grenoble I, 1381 Rue de la Piscine - 38041 Grenoble, France
[4]Institut des Sciences Chimiques de Rennes, Université de Rennes 1, UMR CNRS-UR1 6226, Campus de Beaulieu, Bât 10B, 35042 Rennes Cedex, France
[5]Department of Physics, Nano Functional Materials Technology Centre and Materials Science Research Centre, Indian Institute of Technology, Madras – 600036, India.

**msrrao@iitm.ac.in*

Abstract
Ni doped, Li doped and (Li, Ni) codoped ZnO thin films were successfully grown using pulsed laser deposition technique. Undoped and doped ZnO thin films were investigated using EXAFS and XANES. Preliminary investigation on the Zn K-edge of the undoped and doped ZnO thin films revealed that doping has not influenced the average Zn-Zn bond length and Debye-Waller factor. This shows that both Ni and Li doping does not appreciably affect the average local environment of Zn. All the doped ZnO thin films exhibited more than 50% of substitutional Ni with maximum of 77% for 2% Ni and 2% Li doped ZnO thin film. Contribution of Ni metal to the EXAFS signal clearly reveals the presence of Ni clusters. The Ni-Ni distance in the Ni^0 nano-clusters, which are formed in the film, is shorter with respect to the reference Ni metal foil and the Debye-Waller factor is higher. Both facts perfectly reflect what is expected for metal nanoparticles. At the highest doping concentration (5%), the presence of Li favors the growth of a NiO side phase. Indeed, 2% Ni and 5% Li doped ZnO thin film shows $\%Ni_{sub}$ = 75±11, $\%Ni_{met}$ = 10±8, %NiO = 15±8. XANES studies further confirm that the substitutional Ni is more than 50 % in all the samples. These results explain the observed magnetic properties.

1. Introduction

The interest in simultaneous control of both charge and spin has driven the study of transition metal (TM) ion doping in semiconductor materials to realize room temperature ferromagnetism [1]. In III-V and II-VI semiconductors, fraction of the host cations is substitutionally replaced by TM ions to produce room temperature ferromagnetism. Many groups have convincingly demonstrated spin injection and detection studies using Mn doped GaAs with lateral and horizontal geometry. However, all these demonstrated studies were limited to low temperatures because of the low Curie

temperature (~ 170 K) of (Ga, Mn) As system [2, 3]. Considerable efforts were made to study TM ion doped ZnO, after Dietl *et al*.'s prediction of room temperature ferromagnetism in Mn doped *p*-type ZnO [4]. In Mn doped *p*-ZnO systems, a strong *p-d* hybridization between *p*-states of the valence bands and Mn 3*d* levels results in room temperature ferromagnetism [4]. Later, Sato *et al*. have reported room temperature ferromagnetism in TM ion (V, Cr, Mn, Fe, Co and Ni) doped *n*-type ZnO using *ab initio* calculations [5, 6]. Coey *et al*. have explained room temperature ferromagnetism in TM ion doped ZnO and other oxide systems using bound magnetic polaron (BMP) model and explained the role of oxygen vacancies [7]. Nevertheless, all the above models consider the substitutional TM ions in cation (Zn) sites in ZnO. Recent high resolution microscopy and spectroscopy studies showed that the TM ions form nano-sized metal clusters in the ZnO lattice. By means of X-ray absorption spectroscopy (XAS) and high-resolution transmission electron microscopy (HRTEM), Ney *et al*. have shown Co phase segregation in Co doped ZnO thin films grown by laser-MBE [8]. However, Lu *et al*. showed no evidence of detectable Co metallic clusters using X-ray absorption near edge spectroscopy (XANES) and extended X-ray absorption fine structure (EXAFS) in Co doped and (Co, Ga) codoped ZnO thin films grown by MBE technique that showed room temperature ferromagnetism [9].

Li *et al*. have investigated the Ni doped ZnO polycrystalline powders by means of EXAFS and showed that the Ni atoms are in substitutional position in ZnO lattice [10]. Also Venkataiah *et al*. have reported on the substitution Ni doping in ZnO nanorods using EXAFS and XANES studies [11]. Both the above groups do not show any evidence of metallic Ni clusters in Ni:ZnO systems and concluded that the observed ferromagnetism is intrinsic.

Recently, Zhang *et al*. have studied (Mn, Li), (Mn, Na) and (Mn, K) doped ZnO thin films using XRD and XANES techniques and showed that the doped ZnO films are free from clusters, precipitates and secondary phases [12]. Yan *et al*. have shown using XANES studies that the substitutional position of the Co ions is unchanged before and after annealing in air [13]. Snure *et al*. have reported metallic Ni clusters in PLD deposited Ni:ZnO thin films grown under low oxygen pressure [14]. However, Srivastava *et al*. showed no evidence of metallic Ni clusters in Ni implanted ZnO thin films using XAS [15]. Satyarthi *et al*. have reported both substitutional Ni^{2+} and phase segregated Ni clusters in Ni implanted ZnO thin films [16]. Hence, the origin of ferromagnetism in ZnO is still an open debate, i.e., whether the ferromagnetism is an intrinsic property of the material or it arises from the dopant clusters. When compared with Co doped ZnO thin films, microscopic studies on Ni doped ZnO thin films are scarce. Moreover, theoretical calculations highlighted that co-doping group-I elements with TM ions stabilizes ferromagnetic ordering and increase the Curie temperature [17, 18]. These results motivated us to study the magnetic and microstructural properties of (Li, Ni) codoped ZnO thin films.

Recently, we have shown room temperature ferromagnetism in (Li, Ni) codoped ZnO thin films grown by pulsed laser deposition technique [19, 20]. Moreover, we have demonstrated that the observed ferromagnetic nature does not have any dependence on the charge carrier type, but has a strong dependence on the oxygen vacancies and charge carrier concentration. Our X-ray photoelectron spectroscopy (XPS) studies showed no evidence of metallic Ni clusters in 2% Ni doped ZnO thin films. It is inevitable to investigate the chemical environment of Ni in those ZnO films to further understand the origin of ferromagnetism in these systems. XAS is a powerful tool in the study of the local atomic environment in condensed matter since it couples atomic selectivity

and high resolution at the short distance scale [21-23] and, therefore, it is the particularly suitable to investigate the local chemical environment of Ni in the system, as demonstrated also by previous XAS studies on TM doped ZnO [10, 11, 13, 15]. Hence in this paper, we present a detailed EXAFS and XANES study on the Ni doped and (Li, Ni) codoped ZnO thin films grown by pulsed laser deposition technique.

2. Experimental

ZnO films growth. Undoped, 2 % Ni doped, 2% Li doped and (Li, Ni) codoped ZnO thin films were grown on c-axis sapphire substrates using pulsed laser deposition technique (Nd:YAG laser, λ=355 nm operated at a repetition rate of 10 Hz and laser energy density of 2.7 J/cm^2). The Li concentration in the (Li, Ni) codoped ZnO thin films was varied as 0.5%, 1.0%, 2.0%, 3.0% and 5.0% by maintaining Ni concentration at 2%. Thin films were grown at a substrate temperature of 400 ^{o}C at an oxygen partial pressure of 3.5×10^{-2} mbar, while the base pressure of the chamber was 6.2×10^{-6} mbar. The growth time was 10 min that resulted in 300 nm thick ZnO films.

XAS spectroscopy. X-ray absorption experiments at the Zn (9659 eV) and Ni (8333 eV) K-edges were performed at the BM25A beamline [24] of the ESRF facility. The white beam was monochromatized using a Si(111) double crystal. The ZnO thin films EXAFS spectra were recorded in fluorescence mode, using a multi-element solid state detector; and a cryostat was employed in order to perform measurements at 20 K. The intensity of the incoming beam I_0 was measured using a ionization chamber filled with a partial N_2 pressure adapted to obtain 15% of efficiency at the edge of the two elements. For the reference samples (Ni metal foil and NiO powder), the EXAFS spectra were acquired in transmission mode using a second ionization chamber filled with Ar.

For all fluorescence spectra, the pre-edge region was acquired with an energy step of 10 eV and an integration time of 3 s/point. The edge region was collected using an energy step of 0.3 eV and an integration time of 3 s/point. The EXAFS part of the spectra was collected with a variable sampling step in energy, resulting in a constant sampling step in k-space of $\Delta k = 0.05$ Å^{-1}, up to 16 Å^{-1}, with an integration time of 20 s/point. The extraction of the $\chi(k)$ function was performed using Athena program [25] in the $\Delta k = 2.0$-13.0 Å^{-1} interval. For all samples, five consecutive EXAFS spectra were collected and the corresponding k^2-weighted $\chi(k)$ functions were averaged [26].

EXAFS data analysis has been performed using the Artemis software.[25] Phase and amplitude functions were calculated by FEFF6 code [27] using as input a clusters obtained from XRD data. A parallel analysis has also been performed using the ESTRA-FitEXA code [28] that represents an evolution of the EXAFS data analysis programs developed in the 1980s by the PULS group at the Frascati National Laboratories. Within the associated error bars (that were in general ~30% higher for the ESTRA-FitEXA code), both analysis led to compatible results. For the sake of brevity, only the FEFF6 results are reported.

For the Zn edge, the fits were performed in R-space in the $\Delta R = 1.0$-4.0 Å range resulting in 23 independent points. The single scattering (SS) and the most relevant multiple scattering (MS) paths involving the first shell oxygen atoms and the second shell zinc atoms were included.

For the Ni edge, the fits were performed in R-space in the $\Delta R = 1.2$-3.5 Å range resulting in 16 independent points. In this case, besides the SS and MS already employed for the Zn edge, a SS Ni-Ni path of Ni metal was added in order to fit the contribution of the Ni metal clusters. For the

sample with the higher Li content, which shows an evident NiO contribution, also a Ni-Ni SS path obtained from the NiO was included.

3. Results and discussion

First of all a preliminary investigation of the Zn K-edge was performed in order to understand if the addition of the Ni and Li dopants can have any influence on the average Zn local environment. For instance, some authors reported that Li doping induces a decrease in intensity of the second shell signal and a shortening of the Zn-Zn distance [29]. Considering Figure 1 and Table 1, we can see that in our samples the first and second shell interatomic distances are comparable to those reported in literature for undoped ZnO [29-31]. Therefore the addition of the dopants is not influencing the bond lengths in a significant way and the same happens also for the Debye-Waller factors, confirming that the local environment of Zn is not appreciably modified by the doping.

Table 1. Summary of the parameters optimized in the fitting process of the Zn K-edge EXAFS data (Figure 1). The fits were performed R-space (1.0 − 4.0 Å range) over k^2-weighted FTs of the $\chi(k)$ functions (2.0 − 13.0 $Å^{-1}$ range). In all cases, the correlation between the couples of fitted variables were in the following ranges: 0.80-0.83 between S_0^2 and σ^2_{Zn}; 0.75-0.79 between ΔE and R_{Zn}. All other correlations were below 0.64 in absolute value.

Zn K-edge	ZnO undoped	Li2%	Ni2%	Ni2% - Li5%
R factor	0.03	0.05	0.04	0.04
S_0^2	0.92±0.08	0.9±0.1	0.92±0.09	0.91±0.08
ΔE (eV)	5.3±0.7	5±1	5.5±0.9	5.8±0.8
R_O (Å)	1.95±0.01	1.95±0.01	1.96±0.01	1.96±0.01
σ^2_O ($Å^2 \cdot 10^3$)	4±1	6±2	5±2	4±2
R_{Zn} (Å)	3.222±0.005	3.224±0.007	3.228±0.006	3.232±0.006
σ^2_{Zn} ($Å^2 \cdot 10^3$)	4.3±0.6	3.9±0.7	4.5±0.7	5.1±0.7

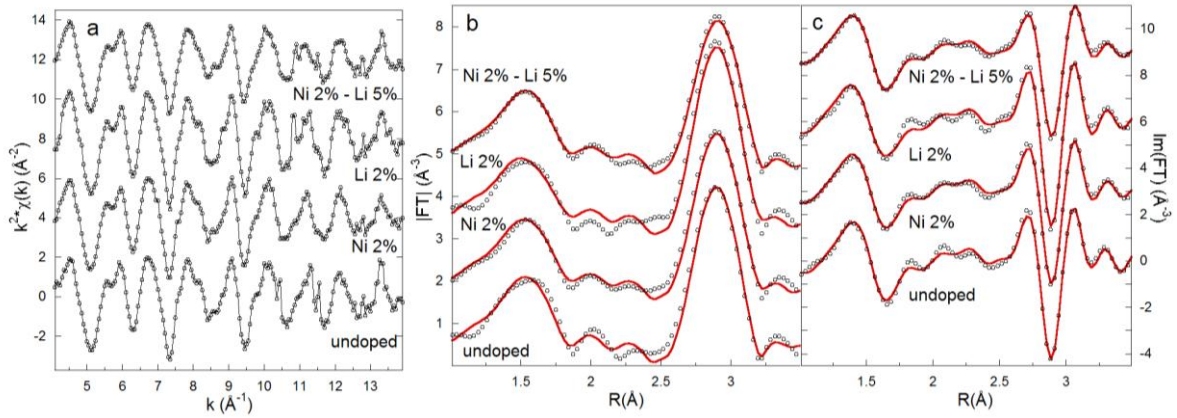

Figure 1. (a) k^2-weighed $\chi(k)$ function of the Zn K-edge for the undoped, Ni2%, Li2% and Ni2%-Li5% ZnO samples. (b) Comparison between experimental data (gray dots) and corresponding best fits (red line) for the phase uncorrected Fourier Transform modulus of the k^2-weighed $\chi(k)$ functions reported in part (a) (vertical translated for clarity). The results of the fits are summarized in Table 1. (c) As part (b) for the Fourier Transform imaginary part.

Moving to the Ni K-edge, we can consider Figure 2a-b-c which compares three doped ZnO films: the complexity of the signal is readily appreciable. In particular, we can see that the Ni K-edge data for the doped samples show a contribution analogous to the Zn K-edge EXAFS signal of the undoped ZnO film (Figure 2d-e-f). This similarity readily suggests the presence of substitutional Ni.

Moreover a contribution of Ni metal to the Ni,Li-ZnO EXAFS signal is clearly visible: in particular the first shell Ni-Ni contribution at about 2.2 Å and the typical triplet of the fcc metals at 3.2, 4.0 and 4.6 Å in the phase uncorrected |FT|. Finally, we can notice that the sample with the higher Li content exhibits also an additional contribution at around 2.4 Å in the phase uncorrected |FT|, which can be ascribed to NiO.

In order to properly fit the data, we employed the single scattering (SS) and the most relevant multiple scattering (MS) paths already used for the Zn edge to model the signal coming from the Ni which is substituting Zn. Moreover, we added the Ni-Ni SS path, obtained from the Ni foil, to fit the contribution deriving from the Ni metal. In order to decrease the number of free parameters, the ΔE for the Ni-Ni SS path was defined as $\Delta E_{met} = \Delta E_{sub} - (E_{NiO}-E_{foil})$, where E_{NiO} is the absorption edge energy for the NiO (8341 eV) and E_{foil} absorption edge energy for the Ni metal (8333 eV). The percentage of substitutional Ni was estimated by imposing that the total amplitude for the two phases is equal to the amplitude of the standards (for both Ni metal and NiO $S_0^2 \sim 0.8$).

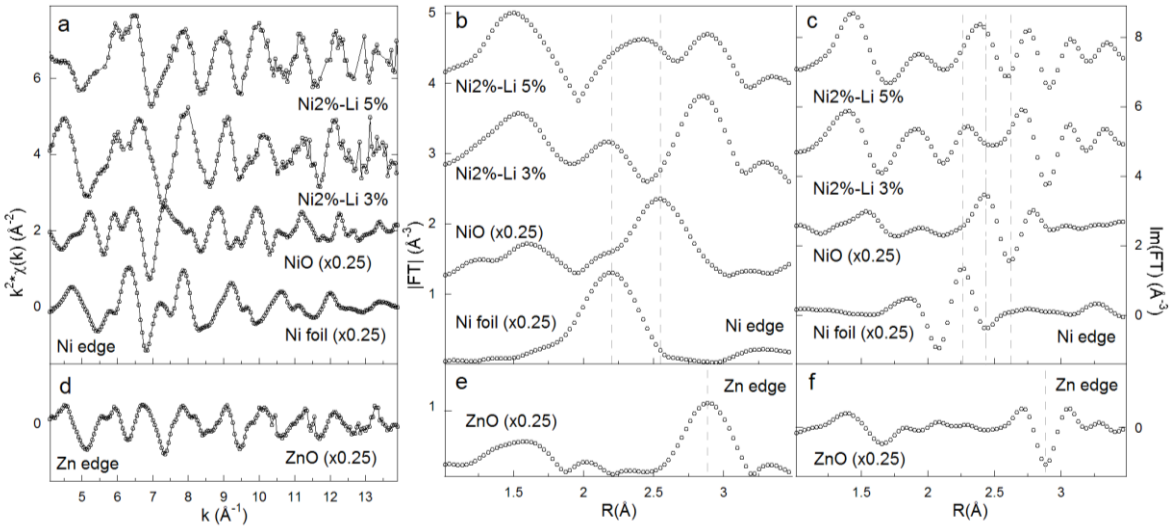

Figure 2. (a) k^2-weighed $\chi(k)$ function of the Ni K-edge for the Ni foil, NiO powder, Ni2%-Li3% , and Ni2%-Li5% ZnO samples. (b) Phase uncorrected Fourier Transform modulus of the k^2-weighed $\chi(k)$ functions reported in part (a) (vertical translated for clarity). (c) As part (b) for the Fourier Transform imaginary part. (d) k^2-weighed $\chi(k)$ function of the Zn K-edge for the undoped ZnO thin film. (e) Phase uncorrected Fourier Transform modulus of the k^2-weighed $\chi(k)$ function reported in part (d). (f) As part (e) for the Fourier Transform imaginary part.

From Table 2 we can see that the Ni-O (R_O) bond length in the substitutional phase is slightly longer with respect to the Zn-O bond length obtained from the Zn K-edge of ZnO (see Table 1). This experimental evidence was already observed in literature [32] and contradicts what can be expected by simply considering the ionic radii of Ni^{2+} and Zn^{2+} ions in tetrahedral coordination (0.55 and 0.60 Å, respectively) [33]. The second shell Ni-Zn (R_{Zn} in Table 2) distances are very similar to the Zn-Zn distances in ZnO (see Table 1).

Concerning the fraction of Ni which is substituting Zn, there is not an evident trend related to the variation of Li content, however the percentage of substitutional Ni is above 50% for all samples. The Ni-Ni distance in the Ni clusters which are formed in the film is shorter with respect to the R_{Ni} measured in the Ni metal foil (2.484±0.003 Å) and the Debye-Waller factor is higher (σ^2 Ni metal = 5.9±0.4 10^{-3}Å^2·). Both facts perfectly reflect what is expected for metal nanoparticles where: (i) the

metal-metal distances of the relevant fraction of surface atoms are shrinked with respect to the bulk metal owing to their coordinative unsaturation; (ii) different local environments result in an higher Debye-Waller factor of static (non thermal) origin, reflecting an higher local disorder [34].

As visible in Figure 2a-b-c, the Ni2%-Li5% sample, which has the highest Li content, shows also a contribution deriving from NiO. We tried to fit this experimental data by adding to the previously presented model also the first four SS contributions of the NiO phase (up to the Ni-Ni one lattice parameter apart) together with the two triangular MS paths involving Ni-O1-O2 and Ni-Ni1-O1 [35, 36]. To limit the number of optimized variables, all the parameters of the new NiO phase were fixed to the values obtained from the EXAFS refinement of the NiO model compound, therefore optimizing only the relative fraction of this phase. As in the previous fits, the sum of the fraction of the three phases was constrained to unit, therefore in this case we optimized the fraction of two phases instead of one, obtaining $\%Ni_{sub}$ = 75±11, $\%Ni_{met}$ = 10±8, %NiO = 15±8. Notwithstanding the use of an additional free parameter, the quality of this fit is slightly poorer (R factor = 0.05), reflecting the difficulties in the joint refinement of three phases (see Figure 3). Within the associated error bars, the refined parameters of both the substitutional and metallic phases agree with those obtained for the other doped samples where the EXAFS data analysis has been less delicate (see Table 2).

Table 2. Summary of the parameters optimized in the fitting of the Ni K-edge EXAFS data (Figure 3). The fits were performed R-space (1.2 – 3.5 Å range) over k^2-weighted FTs of the χ(k) functions (2.0 − 13.0 $Å^{-1}$ range). In all cases, the correlation between the couples of fitted variables were in the following ranges: 0.84-0.79between $\%Ni_{sub}$ and σ^2_{Ni}; 0.82-0.76 between ΔE and R_{Zn}; 0.84 between $\%Ni_{sub}$ and $\%Ni_{met}$ (only for the Ni2% - Li5% sample). All other correlations were below 0.67 in absolute value.

Ni K-edge	Ni2%	Ni2% - Li0.5%	Ni2% - Li1%	Ni2% - Li2%	Ni2% - Li3%	Ni2% - Li5%[b]
R factor	0.03	0.03	0.02	0.04	0.03	0.05
ΔE_{sub} (eV)	1±1	0±2	0±1	0±1	1±1	-4±2
R_O (Å)	1.98±0.02	1.96±0.02	1.97±0.01	1.99±0.02	1.98±0.01	1.96±0.02
σ^2_O ($Å^2 \cdot 10^3$)	5±2	6±2	5±2	5±2	5±2	6±2
R_{Zn} (Å)	3.23±0.01	3.22±0.01	3.22±0.01	3.23±0.01	3.236±0.009	3.25±0.02
σ^2_{Zn} ($Å^2 \cdot 10^3$)	8±1	8±1	8±1	7±1	7±1	11±3
ΔE_{met} (eV)[a]	-7±1	-8±2	-8±1	-8±1	-7±1	-12±4
R_{Ni} (Å)	2.45±0.01	2.44±0.01	2.45±0.01	2.43±0.02	2.46±0.01	2.47±0.03
σ^2_{Ni} ($Å^2 \cdot 10^3$)	10±2	9±1	11±2	11±4	13±2	8±6
$\%Ni_{sub}$	69±7	62±6	59±6	77±8	65±7	75±11

[a]Parameter defined as $\Delta E_{met} = \Delta E_{sub} - (E_{NiO} - E_{foil})$ [b]This fit included three crystal phases: Ni_{sub} = 75±11% , Ni_{met} = 10±8% and NiO = 15±8%

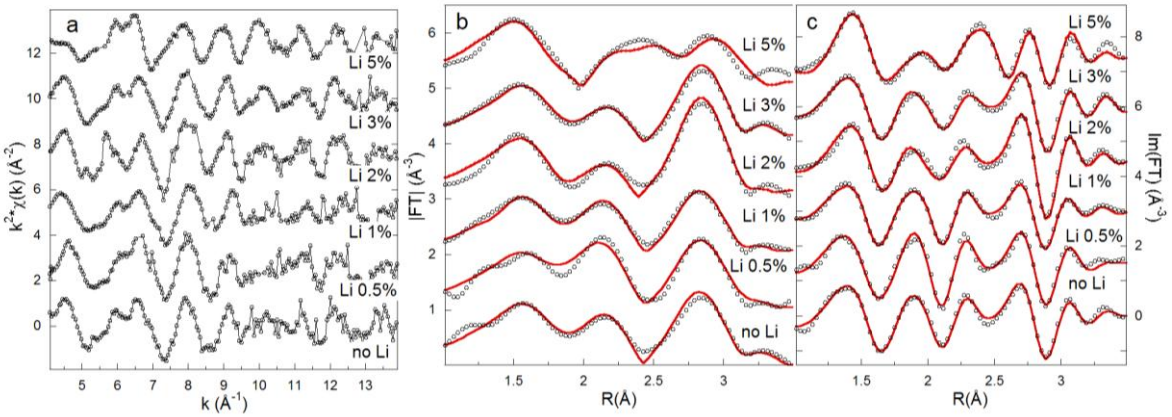

Figure 3. (a) k^2-weighed $\chi(k)$ function of the Ni K-edge for the Ni2%, Ni2%-Li0.5% , Ni2%-Li1%, Ni2%-Li2%, Ni2%-Li3% and Ni2%-Li5% ZnO samples. (b) Comparison between experimental data (gray dots) and corresponding best fits (red line) for the phase uncorrected Fourier Transform modulus of the k^2-weighed $\chi(k)$ functions reported in part (a) (vertical translated for clarity). The results of the fits are summarized in Table 2. (c) As part (b) for the Fourier Transform imaginary part.

Finally, we can consider the XANES region (Figure 4) which is particularly sensitive to the absorber oxidation state [37]. All spectra show a pre-edge peak ascribed to the transition from the 1s core level to bound unoccupied d states near the Fermi level. Its weak intensity is due to the fact that this transition is forbidden by dipole selection rules. However, it is allowed by quadrupole selection rules and can be enhanced also by the hybridization between unoccupied states with p and d character.[38] The pre-edge maximum is followed by the main edge jump, originated by the 1s → 4p dipole allowed transition [39], and then by the white line (WL) at 8343 eV.

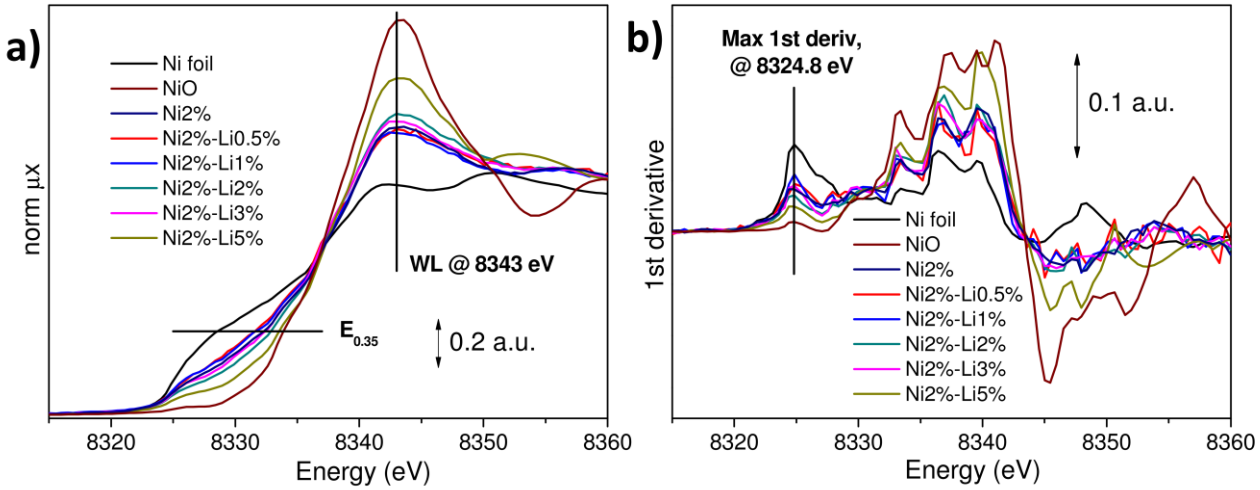

Figure 4. Normalized XANES spectra (a) and corresponding first derivative (b) for all the samples and standards. The different approaches used to estimate the percentage of the substitutional Ni, summarized in Table 3, are reported.

In literature the energy position of the edge and of the pre-edge feature have been found to be linearly correlated to the Ni oxidation state [40-42]. So we can use the XANES spectra to independently estimate the fraction of oxidized (substitutional and eventually NiO) and reduced (metallic) nickel. In order to achieve a more comprehensive picture, we tried different approaches, which are summarized in Table 3. In particular, adapting to this particular case the more frequently used approaches [23, 37, 43-47], we considered: (i) the normalized intensity at the maximum of the first derivative at 8324.8 eV; (ii) the energy position of the point closest to the 0.35 value of normalized intensity ($E_{0.35}$), where the difference in energy position between reduced and oxidized Ni is maximum; (iii) the normalized intensity of the white line at 8343 eV; (iv) a fit of the XANES signal using a linear combination of reference spectra (Figure 5). To obtain the percentage of Ni metal present in the doped samples, we used as reference the spectra of the Ni metal foil and of the Ni2% - Li5% sample, in which the content of Ni clusters is negligible. We tried also to employ the

NiO XANES spectrum as reference for the 0% Ni metal, but the quality of the fits was considerably worse owing to the different coordination of the Ni in the oxide (octahedral vs. tetrahedral).
Considering Table 3, we can see that the values obtained using the different approaches to analyze the XANES data generally show the same trend and confirm that the percentage of substitutional Ni is above 50% for all samples as obtained from the EXAFS analysis. It is worth to note that, for the $E_{0.35}$ method, the measurement resolution is limited by the adopted sampling step of the monochromator (0.3 eV). The percentages of substitutional Ni obtained monitoring the normalized intensity at the maximum of the first derivative show the best agreement with the EXAFS data: the close correlation of this quantity with the Ni metal content was already observed in previous studies [46].

Table 3. Percentage of substitutional Ni in the doped samples obtained considering the normalized intensity at the maximum of the first derivative, the energy position of the point closest to the 0.35 value of normalized intensity ($E_{0.35}$), the normalized intensity of the white line (WL) and a fit using a linear combination of reference spectra (Figure 5). In the last line the values obtained from EXAFS (Table 2) are reported for comparison.

Ni K-edge	Ni2%	Ni2% - Li0.5%	Ni2% - Li1%	Ni2% - Li2%	Ni2% - Li3%
Max 1st deriv.	72	63	50	81	66
$E_{0.35}$	75	61	61	91	84
Max WL	54	52	50	67	60
Linear comb.	63	53	56	73	67
EXAFS	69	62	59	77	65

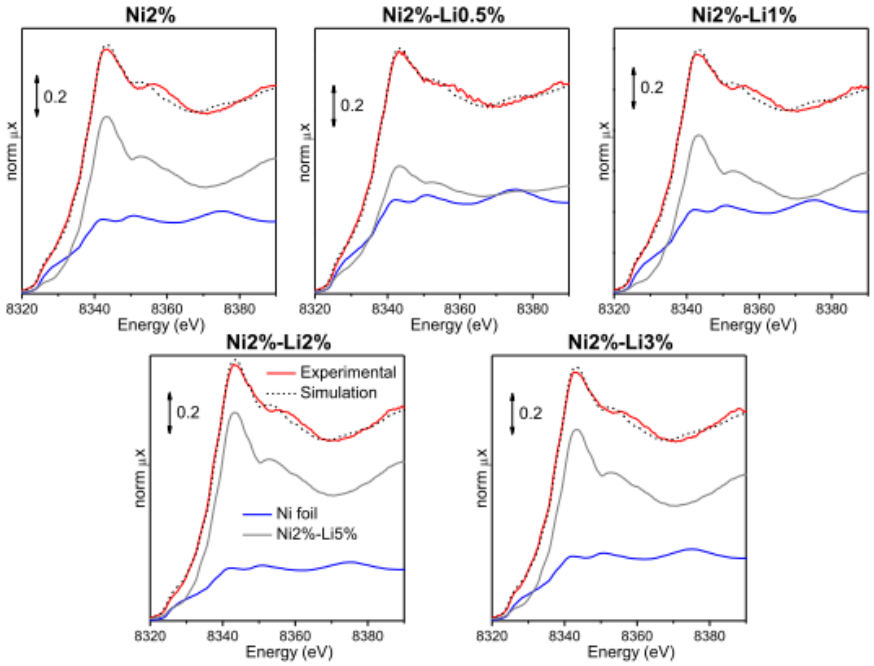

Figure 5. Normalized XANES spectra and best fits of the doped ZnO films together with the spectra of the two model compounds (Ni foil for metallic Ni and Ni2%-Li5% for substitutional Ni) weighted by the corresponding optimized fractions.

4. Conclusions

(Li, Ni) codoped ZnO thin films were grown using pulsed laser deposition technique with a wide range of Li concentrations. Both EXAFS and XANES confirm that more than 50 % of Ni goes into substitutional sites in ZnO with a maximum of 77% for 2% Ni and 2% Li doped ZnO and minimum of 59 % for 2% Ni and 1% Li doped ZnO. Higher Li doped samples showed the presence of NiO phase up to 15±8 %. Evidence of metallic clusters is clearly seen in the EXAFS signals.

The previously observed ferromagnetic signal of 0.12 μ_B/Ni from 2% Ni and 2% Li doped ZnO is very much close to the magnetic moment observed in Ni nanoclusters of size 1.9 nm, embedded in AlN [10, 41]. Considering the fact that only a maximum of 77 % of Ni ions can be substitutionally doped and 23 % (~1/4th) of the Ni may have been found as metallic nanoclusters in 2% Ni and 2% Li doped ZnO, the observed ferromagnetic signals may arise from the Ni clusters in ZnO lattice. Hence our detailed EXAFS and XANES studies confirm that the room temperature ferromagnetic signal from 2% Ni and 2% Li doped ZnO is unlikely to be an intrinsic property of the host lattice and may have solely come from Ni nanoclusters.

Acknowledgements

MSR would like to acknowledge department of science and technology (DST) of India for the financial support (Grant:SR/NM/NAT/02-2005) for the establishment of Nano Functional Materials Technology Centre (NFMTC) at IIT Madras. This collaboration between Torino University and ITT Madras was performed within the MaMaSELF frame (http://www.mamaself.eu/) that supported the stay of MSR in Europe and of LM and CP in India. We are indebted with the whole staff of the ESRF SpLine-BM25A beamline (Spanish CRG), and particularly with Dr. Iván da Silva, for the competent support during the XAS data collection.

References

[1] Macdonald A H, Schiffer P and Samarth N 2005 *Nat. Mater.* **4** 195
[2] Ohno H 1998 *Science* **281** 951
[3] Chiba D, Takamura K, Matsukura F and Ohno H 2003 *Appl. Phys. Lett.* **82** 3020
[4] Dietl T, Ohno H, Matsukura F, Cibert J and Ferrand D 2000 *Science* **287** 1019
[5] Sato K and Katayama-Yoshida H 2000 *Jpn. J. Appl. Phys. Part 2 - Lett.* **39** L555
[6] Sato K and Katayama-Yoshida H 2001 *Physica B* **308** 904
[7] Coey J M D, Venkatesan M and Fitzgerald C B 2005 *Nat. Mater.* **4** 173
[8] Ney A, Opel M, Kaspar T C, Ney V, Ye S, Ollefs K, Kammermeier T, Bauer S, Nielsen K W, Goennenwein S T B, Engelhard M H, Zhou S, Potzger K, Simon J, Mader W, Heald S M, Cezar J C, Wilhelm F, Rogalev A, Gross R and Chambers S A 2010 *New J. Phys.* **12** 16
[9] Lu Z L, Hsu H S, Tzeng Y H and Huang J C A 2009 *Appl. Phys. Lett.* **94** 152507
[10] Li B B, Xiu X Q, Zhang R, Tao Z K, Chen L, Xie Z L, Zheng Y D and He B 2006 *Chin. Phys. Lett.* **23** 907
[11] Venkataiah G, Huang M R S, Su H L, Liu C P and Huang J C A 2010 *J. Phys. Chem. C* **114** 16191
[12] Zhang L Q, Zhang Y Z, Ye Z Z, Lu J G, Lu B and He B 2012 *J. Appl. Phys.* **111** 123524
[13] Yan W S, Jiang Q H, Sun Z H, Yao T, Hu F C and Wei S Q 2010 *J. Appl. Phys.* **108** 013901
[14] Snure M, Kumar D and Tiwari A 2009 *Appl. Phys. Lett.* **94** 012510
[15] Srivastava P, Ghosh S, Joshi B, Satyarthi P, Kumar P, Kanjilal D, Buerger D, Zhou S, Schmidt H, Rogalev A and Wilhelm F 2012 *J. Appl. Phys.* **111** 013715
[16] Satyarthi P, Ghosh S, Pandey B, Kumar P, Chen C L, Dong C L, Pong W F, Kanjilal D, Asokan K and Srivastava P 2013 **113** 183708
[17] Petit L, Schulthess T C, Svane A, Szotek Z, Temmerman W M and Janotti A 2006 *Phys. Rev. B* **73** 045107
[18] Pei G Q, Xia C T, Wu B, Wang T, Zhang L L, Dong Y J and Xu J 2008 *Comput. Mater. Sci.* **43** 489
[19] Kumar E S, Venkatesh S and Rao M S R 2010 *Appl. Phys. Lett.* **96** 232504

[20] Kumar E S, Chatterjee J, Rama N, DasGupta N and Rao M S R 2011 *ACS Appl. Mater. Interfaces* **3** 1974
[21] Boscherini F in *Characterization of Semiconductor Heterostructures and Nanostructures (Second Edition)* (Eds.: C. Lamberti, G. Agostini), Elsevier, Amsterdam, **2013**, pp. 259
[22] Mino L, Agostini G, Borfecchia E, Gianolio D, Piovano A and Lamberti C 2013 *J. Phys. D: Appl. Phys.* invited topical Review (submitted)
[23] Bordiga S, Groppo E, Agostini G, van Bokhoven J A and Lamberti C 2013 *Chem. Rev.* **113** 1736
[24] Castro G R 1998 *J. Synchrot. Radiat.* **5** 657
[25] Ravel B and Newville M 2005 *J. Synchrot. Radiat.* **12** 537
[26] Lamberti C, Bordiga S, Arduino D, Zecchina A, Geobaldo F, Spano G, Genoni F, Petrini G, Carati A, Villain F and Vlaic G 1998 *J. Phys. Chem. B* **102** 6382
[27] Ankudinov A L, Ravel B, Rehr J J and Conradson S D 1998 *Phys. Rev. B* **58** 7565
[28] Meneghini C, Bardelli F and Mobilio S 2012 *Nucl. Instrum. Methods Phys. Res. Sect. B* **285** 153
[29] Tsai S Y, Hon M H and Lu Y M 2011 *J. Phys. Chem. C* **115** 10252
[30] Mokili B, Charreire Y, Cortes R and Lincot D 1996 *Thin Solid Films* **288** 21
[31] Phan T L, Zhang P, Yang D S, Nghia N X and Yu S C 2011 *J. Appl. Phys.* **110** 6
[32] Li B B, Xiu X Q, Zhang R, Tao Z K, Chen L, Xie Z L, Zheng Y D and Xie Z 2006 *Mater. Sci. Semicond. Process* **9** 141
[33] Shannon R D 1976 *Acta Cryst. A* **32** 751
[34] Groppo E, Liu W, Zavorotynska O, Agostini G, Spoto G, Bordiga S, Lamberti C and Zecchina A 2010 *Chem. Mat.* **22** 2297
[35] Lamberti C, Groppo E, Prestipino C, Casassa S, Ferrari A M, Pisani C, Giovanardi C, Luches P, Valeri S and Boscherini F 2003 *Phys. Rev. Lett.* **91** 046101
[36] Groppo E, Prestipino C, Lamberti C, Luches P, Giovanardi C and Boscherini F 2003 *J. Phys. Chem. B* **107** 4597
[37] Borfecchia E, Mino L, Gianolio D, Groppo C, Malaspina N, Martinez-Criado G, Sans J A, Poli S, Castelli D and Lamberti C 2012 *J. Anal. At. Spectrom.* **27** 1725
[38] Yamamoto T 2008 *X-Ray Spectrom.* **37** 572
[39] Mino L, Colombo V, Vitillo J G, Lamberti C, Bordiga S, Gallo E, Glatzel P, Maspero A and Galli S 2012 *Dalton Trans.* **41** 4012
[40] Mansour A N and Melendres C A 1995 *Physica B* **208** 583
[41] Mansour A N and Melendres C A 1998 *J. Phys. Chem. A* **102** 65
[42] Woolley R J, Illy B N, Ryan M P and Skinner S J 2011 *J. Mater. Chem.* **21** 18592
[43] Lamberti C, Bordiga S, Bonino F, Prestipino C, Berlier G, Capello L, D'Acapito F, Xamena F and Zecchina A 2003 *Phys. Chem. Chem. Phys.* **5** 4502
[44] Lamberti C, Prestipino C, Bonino F, Capello L, Bordiga S, Spoto G, Zecchina A, Moreno S D, Cremaschi B, Garilli M, Marsella A, Carmello D, Vidotto S and Leofanti G 2002 *Angew. Chem.-Int. Ed.* **41** 2341
[45] Le Toquin R, Paulus W, Cousson A, Prestipino C and Lamberti C 2006 *J. Am. Chem. Soc.* **128** 13161
[46] Nietubyc R, Czerwosz E, Diduszko R, Dluzewski P, Kozlowski M and Welter E 2009 *J. Alloy. Compd.* **484** 896
[47] Piovano A, Agostini G, Frenkel A I, Bertier T, Prestipino C, Ceretti M, Paulus W and Lamberti C 2011 *J. Phys. Chem C* **115** 1311